85

# On the spatial evolution of centrifugal instabilities within curved incompressible mixing layers

## By S. R. OTTO[1], T. L. JACKSON[2] AND F. Q. HU[3]

[1]School of Mathematics and Statistics, The University of Birmingham, Edgbaston, Birmingham, B15 2TT, UK

[2]ICASE, Mail Stop 132 C, NASA Langley Research Center, Hampton, VA 23681–0001, USA

[3]Department of Mathematics and Statistics, Old Dominion University, Norfolk, VA 23529, USA

It is known that certain configurations which possess curvature are prone to a class of instabilities which their 'flat' counterparts will not support. The main thrust of the study of these centrifugal instabilities has concentrated on curved solid boundaries and their effect on the fluid motion. In this article attention is shifted towards a fluid–fluid interface observed within a curved incompressible mixing layer. Experimental evidence is available to support the conjecture that this situation may be subject to centrifugal instabilities. The evolution of modes with wavelengths comparable with the layer's thickness is considered within moderately curved mixing layers. The high Taylor/Görtler number régime is also discussed which characterizes the ultimate fate of the modes.

## 1. Introduction

The understanding of the dynamics involved in mixing layers is crucial in many physical problems. The necessarily inflectional profile can support inviscid modes which are known to be responsible for many of the structures that are observed. The work of Michalke (1964,1965) describes the temporal and spatial linear stability of incompressible shear layers. The catalogue of work concerning this situation is immense; it suffices to say that the problem has been studied by many prolific authors. However, one physical process that has received relatively little attention is the subject tackled herein: that is, the effect of centreline curvature on the stability of mixing layers.

Most of the work to date concerning this particular subject has considered turbulent mixing layers within experimental contexts, namely: Margolis & Lumley (1965), Wyngaard *et al.* (1968), Castro & Bradshaw (1976), Wang (1984), Karasso & Mungal (1990,1991), LeBoeuf (1991) and more recently Plesniak, Mehta & Johnston (1994). This experimental work has demonstrated that, if the mixing layer curves towards the faster stream, the situation can support longitudinal vortices. Here we complement the experimental work by examining, both theoretically and by direct numerical solution, the evolution of Görtler vortices with order-one wavenumbers, within situations typified by order-one Görtler numbers.

Since the early work of Taylor (1923) and Görtler (1940) there has been a host of

articles devoted to the study of centrifugal instabilities. Taylor (1923) demonstrates that the flow between two concentric cylinders is susceptible to toroidal modes when the inner cylinder rotates at an angular velocity with a value within a certain interval. In an exterior problem, namely the flow over a curved plate, Görtler showed that the boundary layer on a concave plate will support longitudinal vortices. These modes remain within the boundary layer and have spanwise wavelengths comparable with the boundary layer thickness. It is known that the evolution of Görtler vortices is strongly dependent on their initial form and position, and the thickening of the boundary layer plays a critical role in their fate. It was in the work of Hall (1983) that the full parabolic linear Görtler equations were solved numerically. It was shown that it is essential for the layer's evolution to be included in the analysis. A starting condition was used which was consistent with the equations and the solution was progressed downstream. It was demonstrated that the structure of the mode depended heavily on the streamwise position at which the disturbance was imposed. The characteristics of the modes, independent of initial form and position, eventually coalesce, so that the idea that one can exploit a far downstream asymptotic structure is an option. This involves considering high-wavenumber vortices in a high-Görtler-number situation; this analysis was originally given in Hall (1982). Here, we initially consider the structure of Görtler vortices within spatially evolving mixing layers with order-one Görtler numbers. These calculations allow one to predict the decay, growth and subsequent decay of the vortices, as they evolve downstream. The main aims of this article are to demonstrate that the curved mixing layer can support centrifugal modes for a finite downstream distance and to provide a description of their structure.

As mentioned previously, the consideration of high centrifugal parameter asymptotics can be very revealing. The high Taylor/Görtler number régime is split into two distinct problems: firstly the inviscid modes and secondly the right-hand branch modes. The former of these problems is pertinent when a mode with spanwise wavelength comparable with the boundary layer thickness is introduced into a high Taylor/Görtler number situation. The second problem occurs when a mode has a high wavenumber (i.e. short wavelength) and it attains a neutral state. As a layer thickens the centrifugal modes are known to maintain their wavelength, hence the local wavelength actually decreases. As the wavenumber of the modes increases in the inviscid problem we should match directly onto the small-wavenumber limit of the right-hand branch calculation. It is in this intermediate régime that the most unstable linear mode is encountered. In the Görtler problem this régime contains a singularity in the growth rate, due to the fact that the mode is driven to the wall where the basic velocity becomes zero (Denier, Hall & Seddougui 1991). In the current case the velocity is non-zero where the mode resides and hence we do not expect to find this significantly more dangerous mode.

Two recent articles have tackled the problem analytically, concerning themselves with the fate of order-one-wavenumber vortices within highly curved situations. Both of these articles are limited in scope, since they use a hyperbolic tangent profile to model the underlying basic flow, which ignores the non-parallel nature of the mean flow, necessary for the study of Görtler vortices. The assumption of a parallel flow then allows the investigation of a local eigenvalue problem, in which the wave in the streamwise direction is assumed periodic. For this case a Rayleigh equation can be derived, modified by curvature. The local eigenvalue problem can then be solved in order to determine the possible growth rates of the modes. Liou (1994) is devoted to the effect of curvature on inflectional modes and also identifies three-dimensional steady centrifugal modes. Hu, Otto & Jackson (1994) is concerned both with that

problem and also the question of the pure inviscid Görtler problem, given in Drazin & Reid (1979). We can summarize the findings of Hu *et al.* (1994) as follows: (i) the effect of centreline curvature on the Rayleigh modes appears to be minimal, and (ii) the presence of curvature permits an unstable three-dimensional mode which will become the prominent mode as the scaled streamwise wavelength decreases (this corresponds to reverting to the centrifugal case for which this wavelength is zero). The apparent features of the inviscid Görtler problem can be described as that, when the centreline curves into the faster stream, the situation can support a family of unstable modes. However, if the centreline curves into the slower stream the situation is totally stable to inviscid Görtler modes.

In the conventional Görtler problem the basic state is unaffected by the situation's curvature and this is also true in our case. However, unlike the Görtler case in which the basic state is given by a Blasius profile, we shall assume that the basic state is given by the Lock (1951) profile in which the normal velocity is taken to be zero at the centreline. For comparison purposes, we shall also report selected results for the hyperbolic tangent profile; however, it must be remembered that the spatial evolution of the layer is crucial and thus it is not sufficient to use the hyperbolic tangent profile. In our discussion of the high-Görtler-number modes, we shall comment on the difference between the two profiles. This is highlighted by considering certain characteristics of the modes as the disparity between the two stream speeds increases.

The remainder of this article is structured as follows: in §2 we formulate the problem at hand, then in §§3 and 4 we consider the high-Görtler-number problems and their subsequent matching. In §5 the numerical methods used to solve the order-one wavenumber problem are described in brief. In §6 the results of the numerical calculations are given and finally in §7 some conclusions are drawn.

## 2. Formulation

The problem considered here is the stability of an incompressible steady laminar mixing layer which lies between two streams with different speeds in a channel with curvature $\chi(x)$. A schematic is given in figure 1. The upper stream is travelling at $U_0$ and the lower stream at $\beta_u U_0$. We assume that the Reynolds number $Re = U_0 d/\nu$ of the situation is large, where $d = R_2 - R_1$ is the height of the channel, assumed to be constant, and $\nu$ is the kinematic viscosity. Here, $R_2$ is the radius of the outer wall and $R_1$ is the radius of the inner. We consider the incompressible Navier–Stokes equations in cylindrical coordinates, such that the mixing layer lies along $r^* = R_1 + d/2 + dy^*$. The velocities are non-dimensionalized by $U_0$ and lengths by $d$. We assume that the local curvature of the channel $\delta = d/R_1$ is small. The non-dimensional steady equations, assuming $\delta \ll 1$, are thus given by

$$\frac{\partial u}{\partial x} + \frac{\partial v}{\partial y} + \frac{\partial w}{\partial z} = 0,$$

$$u\frac{\partial u}{\partial x} + v\frac{\partial u}{\partial y} + w\frac{\partial u}{\partial z} = -\frac{\partial p}{\partial x} + \frac{1}{Re}\nabla^2 u,$$

$$u\frac{\partial v}{\partial x} + v\frac{\partial v}{\partial y} + w\frac{\partial v}{\partial z} - \chi\delta u^2 = -\frac{\partial p}{\partial y} + \frac{1}{Re}\nabla^2 v,$$

$$u\frac{\partial w}{\partial x} + v\frac{\partial w}{\partial y} + w\frac{\partial w}{\partial z} = -\frac{\partial p}{\partial z} + \frac{1}{Re}\nabla^2 w,$$
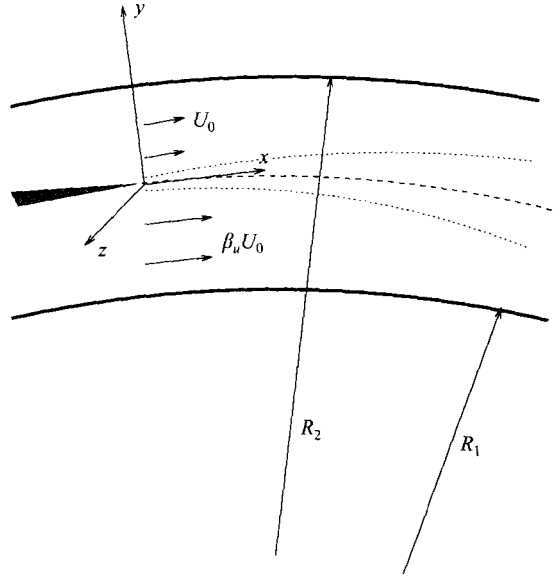
FIGURE 1. Schematic of the flow.

where $\nabla^2$ is the three-dimensional Laplacian operator. We assume that the mixing layer is confined to a small region about $y = 0$, and hence rescale the velocity components $(v, w)$ and coordinates $(y, z)$ by $Re^{-1/2}$. This spanwise scaling is used since we know the vortices have wavelengths commensurate with the layer's thickness. We write the flow field as a sum of the mean flow and its perturbation

$$q = \left(\bar{u}, Re^{-1/2}\bar{v}, 0, 1\right) + \Delta \left(\tilde{U}(x, y), Re^{-1/2}\tilde{V}(x, y), Re^{-1/2}\tilde{W}(x, y), Re^{-1}\tilde{P}(x, y)\right) e^{ikz},$$

where $k$ is the wavenumber in the $z$-direction. The parameter $\Delta$ is vanishingly small so that the resulting analysis is linear and we may discard terms proportional to $\Delta^2$.

We shall focus on two standard models for the mean flow. The first is the Lock model, with the velocity components given by

$$\bar{u} = f'(\eta), \quad \bar{v} = \frac{1}{(2x)^{1/2}} \left(\eta f' - f\right)$$

where

$$f''' + f f'' = 0, \quad f'(\infty) = 1, \quad f(0) = 0, \quad f'(-\infty) = \beta_u,$$

and $\eta$ is the similarity variable $y/(2x)^{1/2}$. This model takes into account the non-parallel nature of the mean flow, necessary for the study of Görtler vortices. The second model involves approximating the mean velocity profile by a hyperbolic tangent

$$\bar{u} = \tfrac{1}{2}\left(1 + \beta_u + (1 - \beta_u) \tanh\eta\right), \quad \bar{v} = 0.$$

We will call this approximation the Tanh model. Most of the results that will be presented below are for the Lock model, but we include some discussion for the Tanh model since it is a standard approximation to the mixing layer. It is worth noting that the Tanh model is not a solution of the basic equations. Since $\bar{u}_x \neq 0$ and $\bar{v} = 0$ it even contradicts the equation of continuity. This model will only be used for the local eigenvalue problems, and it will be shown that, even here, it produces different results.

The perturbation equations are given by

$$\mathscr{L}\left(\frac{\partial^2}{\partial y^2} - k^2\right)\tilde{V} - G\chi k^2 \bar{u}\tilde{U} + 2\frac{\partial^2 \tilde{U}}{\partial x \partial y}\frac{\partial \bar{u}}{\partial x} + 2\frac{\partial \bar{U}}{\partial x}\frac{\partial^2 \bar{u}}{\partial x \partial y}$$

$$+ \tilde{U}\frac{\partial^3 \bar{u}}{\partial x^2 \partial y} + \frac{\partial \tilde{V}}{\partial x}\frac{\partial^2 \bar{u}}{\partial y^2} + \frac{\partial \tilde{V}}{\partial y}\frac{\partial^2 \bar{u}}{\partial x \partial y} + \tilde{V}\frac{\partial^3 \bar{u}}{\partial x \partial y^2} + \frac{\partial \bar{v}}{\partial x}\frac{\partial^2 \tilde{U}}{\partial y^2}$$

$$- \frac{\partial \bar{v}}{\partial y}\frac{\partial^2 \tilde{V}}{\partial y^2} + k^2 \tilde{U}\frac{\partial \bar{v}}{\partial x} + k^2 \tilde{V}\frac{\partial \bar{v}}{\partial y} = 0 \qquad (2.1a)$$

and

$$\mathscr{L}\left(\tilde{U}\right) = \frac{\partial \bar{u}}{\partial x}\tilde{U} + \frac{\partial \bar{u}}{\partial y}\tilde{V}, \qquad (2.1b)$$

where the differential operator $\mathscr{L}$ is given by

$$\mathscr{L} \equiv \frac{\partial^2}{\partial y^2} - k^2 - \bar{u}\frac{\partial}{\partial x} - \bar{v}\frac{\partial}{\partial y}.$$

These equations have the opposite sign for the Görtler term when compared to the conventional Görtler problem owing to the choice of the coordinate system. The Görtler number $G$ is equal to $2\delta Re^{1/2}$ and it is held fixed at an order-one value as $Re \to \infty$ and $\delta \to 0$. We shall shortly consider the limit $G \to \infty$ (but still less than the square root of the Reynolds number). The appropriate boundary conditions are

$$\tilde{U}, \quad \tilde{V}, \quad \frac{\partial \tilde{V}}{\partial y} \quad \to 0 \quad \text{as} \quad y \to \pm\infty. \qquad (2.1c)$$

The numerical and asymptotic solution to the above system is considered in the following sections.

## 3. Viscous right-hand branch modes

It is known that as a Görtler vortex progresses downstream it maintains its spanwise wavelength, and hence the local wavenumber, $kx^{1/2} = k_x$, increases. Also the local Görtler number, $G\chi x^{3/2} = G_x$ increases, and hence it is pertinent to consider a high-Görtler-number calculation. As $G \to \infty$ it is known that $k \sim G^{1/4}$ (if $\chi \sim x^{1/2}$) near the right-hand branch of the neutral curve. For simplicity we shall absorb the leading-order curvature term $\chi_0$ in the Görtler number. In this régime it is known that the mode becomes localized within a thin layer of thickness $k^{-1/2}$ situated at $\bar{y}$ say, Hall (1982). We introduce a layer variable and relevant disturbances quantities so that

$$y = \bar{y} + k^{-1/2}\psi, \quad \tilde{U} = \left(\tilde{U}_0 + k^{-1/2}\tilde{U}_1 + \cdots\right)E \quad \text{and} \quad \tilde{V} = k^2\left(\tilde{V}_0 + k^{-1/2}\tilde{V}_1 + \cdots\right)E,$$

where $E = \exp\left[k^2 \int \left(\beta_0 + k^{-1/2}\beta_1 + \cdots\right)\mathrm{d}x\right]$ and again we are considering steady modes. Since we wish to move away from the neutral curve we also expand $G$ in terms of $k$, so that

$$G = k^4\left[G_0 + k^{-1/2}G_1 + \cdots\right].$$

Substituting these forms into the governing equations and combining the streamwise and normal momentum equations at zeroth and first order, it is found that

$$(\bar{u}_0\beta_0 + 1)^2 + \bar{u}_0\bar{u}_1 G_0 = 0 \qquad (3.1)$$
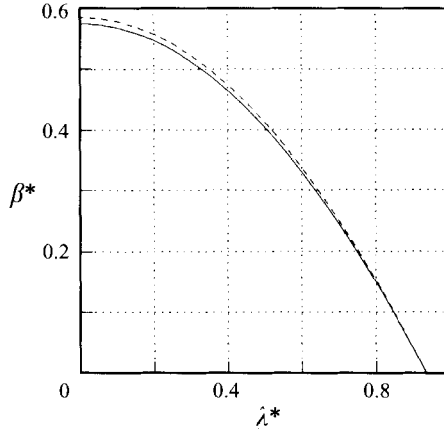
FIGURE 2. Variation of the scaled growth rate $\beta^*$ with the scaled wavenumber $\lambda^*$ with $\beta_u = 2$ (solid line – Lock, dashed line – Tanh).

and

$$2\beta_0 \bar{u}_1 \left(\beta_0 \bar{u}_0 + 1\right) + G_0 \left(\bar{u}_0 \bar{u}_2 + \bar{u}_1^2\right) = 0, \qquad (3.2)$$

where we have expanded $\bar{u}$ locally using a conventional Taylor series as

$$\bar{u} = \bar{u}_0(x) + k^{-1/2}\psi\bar{u}_1(x) + k^{-1}\frac{\psi^2}{2}\bar{u}_2(x) + \cdots.$$

The consistency conditions given by (3.1) and (3.2) provide the growth rate and location of the mode, namely $\beta_0$ and $\bar{y}$. Transforming these conditions to the similarity variables we have

$$\left(\beta^* f' + (\lambda^*)^2\right)^2 + f'f'' = 0, \qquad (3.3)$$

and

$$2\beta^* f'' \left(\beta^* f' + (\lambda^*)^2\right) + (f'f'')' = 0, \qquad (3.4)$$

where $\lambda = G_0^{-1/4}$, with $\lambda$ and $\beta_0$ scaled as

$$\beta_0 = \frac{\beta^* G_0^{1/2}}{(2x)^{1/4}} \qquad \text{and} \qquad \lambda = \frac{\lambda^*}{(2x)^{1/8}}.$$

Note that since $f' = \bar{u}$ is positive thoughout the region the condition (3.1) (and hence (3.3)) requires that $f'' < 0$ at $\bar{\eta} = \bar{y}/(2x)^{1/2}$, that is $\bar{u}_y$ must be negative and hence the lower stream must be faster, hence $\beta_u > 1$ (the centreline curves into the faster stream). Initially we restrict our attention to the case with $\beta_u = 2$. By solving (3.3) and (3.4) it is possible to determine $\beta^*$ as a function of $\lambda^*$ and this is shown for both the Tanh and Lock profiles in figure 2. As $\lambda^* \to 0$, which corresponds to tending towards the inviscid régime, both models predict that $\beta^*$ tends to a constant, 0.585786 for the Tanh model and 0.575432 for the Lock model. We shall shortly see how this matches directly onto the inviscid modes (discussed in the next section). We shall also discuss how the level changes with $\beta_u$. If we concern ourselves with the neutral mode, that is when $\beta^* = 0$, the location of the layer is given by the location at which $(f'f'')'$ is zero (refer to (3.4)) and $\lambda^*$ can be found using the relationship

$$\lambda_N^* = (-f'f'')^{1/4}. \qquad (3.5)$$

For $\beta_u = 2$ with the Tanh model we find that $\eta_N = -0.15595$ yielding $\lambda_N^* = 0.9369$
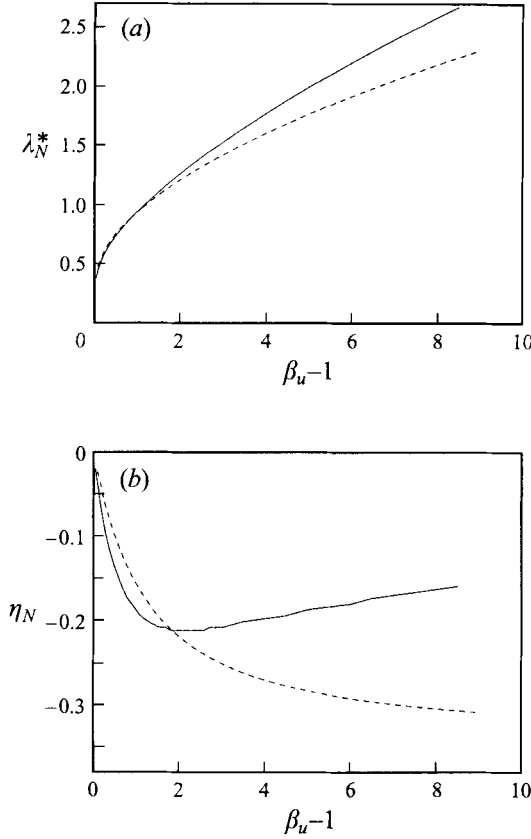
FIGURE 3. (*a*) Variation of $\lambda_N^*$ with $\beta_u$ and (*b*) variation of $\eta_N$ with $\beta_u$ (solid line – Lock, dashed line – Tanh).

and for the Lock profile $\lambda_N^*$ is essentially unaltered (0.9370), but $\eta_N \sim -0.1874$ (that is slightly further out towards the faster stream). In figure 3 we show the effect of changing $\beta_u$ on $\eta_N$ and $\lambda_N^*$. For the Tanh model we can show that

$$\eta_N = \operatorname{arctanh}\left(\frac{\beta_u + 1 - 2(\beta_u^2 - \beta_u + 1)^{1/2}}{3(\beta_u - 1)}\right) \tag{3.6}$$

and from (3.5)

$$\lambda_N^* = \frac{6^{1/4}}{3}\left(\frac{2\beta_u^3 - 3\beta_u^2 - 3\beta_u + 2 + (2\beta_u^2 - 2\beta_u + 2)(\beta_u^2 - \beta_u + 1)^{1/2}}{\beta_u - 1}\right)^{1/4}.$$

This shows quite clearly that as $\beta_u$ increases, $\lambda_N^* \to \beta_u^{1/2}$. This implies that as the disparity between the stream speeds increases a greater range of wavenumbers is unstable. This is also observed in the Lock problem, so that the right-hand branch of the neutral curve moves to the right as $\beta_u$ increases. In figure 3 the dashed lines are the analytic Tanh results and the solid lines are the numerical Lock results. As $\beta_u$ increases the location of the neutral mode for the Lock profile comes back in towards the centreline, whereas in the Tanh model it tends to $\operatorname{arctanh}(-\frac{1}{3}) = \log 1/\sqrt{2} \sim -0.346$. This may be due to the fact that as $\beta_u$ increases the effective width of the mixing
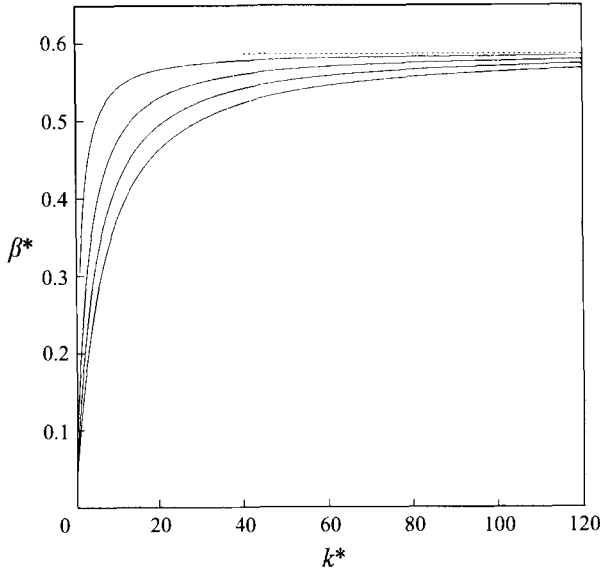
FIGURE 4. Inviscid growth rates for the first four modes with $\beta_u = 2$ and for the Tanh model (asymptote shown as dashed line).

layer narrows in the Lock profile, whereas it remains constant in the more artificial Tanh model.

At the next order the correction to the growth rate is given by

$$\beta_1 = -\frac{\bar{u}_1 G_1}{2(\bar{u}_0\beta_0 + 1)} = -\frac{\bar{u}_1 G_1 \lambda^4}{2(-\bar{u}_0\bar{u}_1)^{1/2}},$$

which tends to zero as $\lambda \to 0$. At the next order the leading-order eigenfunctions are determined, which satisfy a parabolic cylinder equation as is the case in the Görtler problem discussed in Hall (1982).

## 4. Inviscid modes

Denier *et al.* (1991) have shown that the proper expansion of $\tilde{U}$ and $\tilde{V}$ as $G \to \infty$ with $k = O(1)$ is given by

$$\tilde{U} = \exp(G^{1/2} \int \beta dx) / \left( U_0(x, y) + G^{-1/2} U_1(x, y) + \cdots \right),$$

$$\tilde{V} = G^{1/2} \exp(G^{1/2} \int \beta dx) \left( V_0(x, y) + G^{-1/2} V_1(x, y) + \cdots \right),$$

where $\beta$ is the growth rate in the streamwise direction. Substituting into the governing equations yields, at leading order, the system

$$\beta \bar{u} U_0 + \frac{\partial \bar{u}}{\partial y} V_0 = 0, \qquad \beta \left( \frac{\partial^2 \bar{u}}{\partial y^2} - \bar{u}\frac{\partial^2}{\partial y^2} + k^2 \bar{u} \right) V_0 - k^2 \bar{u} U_0 = 0.$$

This system can be rewritten to eliminate $U_0$, yielding

$$-\beta^2 \bar{u} \left( \frac{\partial^2}{\partial y^2} - k^2 - \frac{1}{\bar{u}}\frac{\partial^2 \bar{u}}{\partial y^2} \right) V_0 = -k^2 \frac{\partial \bar{u}}{\partial y} V_0.$$

The appropriate boundary conditions are $V_0 \to 0$ as $y \to \pm\infty$, which correspond to the mode being confined to the layer. Since $\bar{u}$ is given in terms of the similarity

Mode 1

Mode 2

Mode 3

Mode 4
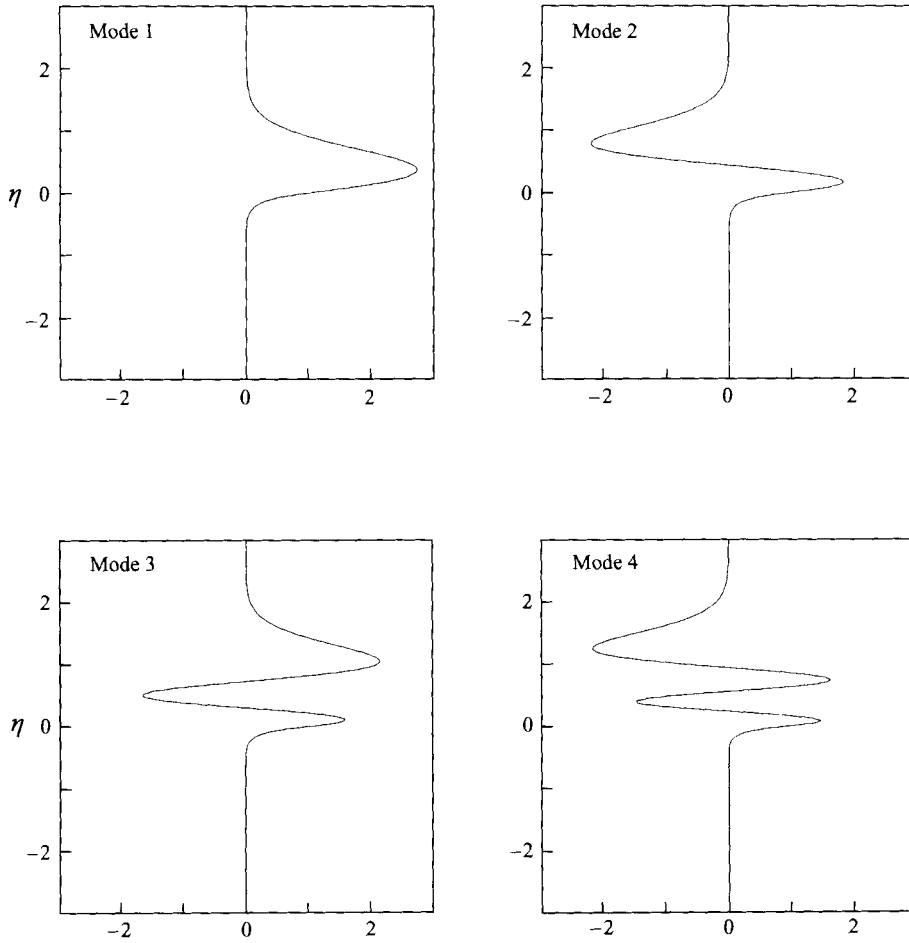
FIGURE 5. Eigenmodes for the first four inviscid modes with $\beta_u = 2$ and for the Tanh model (with $k^* = 6$).

variable $\eta$, it is convenient to transform the above equation, resulting in

$$-\beta^{*2} f' \left( \frac{\partial^2}{\partial \eta^2} - k^{*2} - \frac{f'''}{f'} \right) V_0 = -k^{*2} f'' V_0, \tag{4.1}$$

where

$$k = \frac{k^*}{(2x)^{1/2}}, \quad \beta = \frac{\beta^*}{(2x)^{1/4}}.$$

The above equation was solved numerically for the Tanh model only, using a fourth-order Runge–Kutta technique, shooting in from $\eta = \pm\infty$ and matching the function and its derivative at $\eta = 0$. These results were checked using a fourth-order finite difference scheme. A stretched grid was used to reduce the number of points needed to retain sufficient accuracy. The results presented henceforth in this section are given for the case $\beta_u = 2$, in which the mixing layer curves into the fast stream. It was found, as was to be expected, that for values of $\beta_u$ less than unity there were no unstable vortex modes. The spatial growth rates for the first four modes are given in figure 4, and the eigenforms of these modes are given in figure 5. Upon comparing
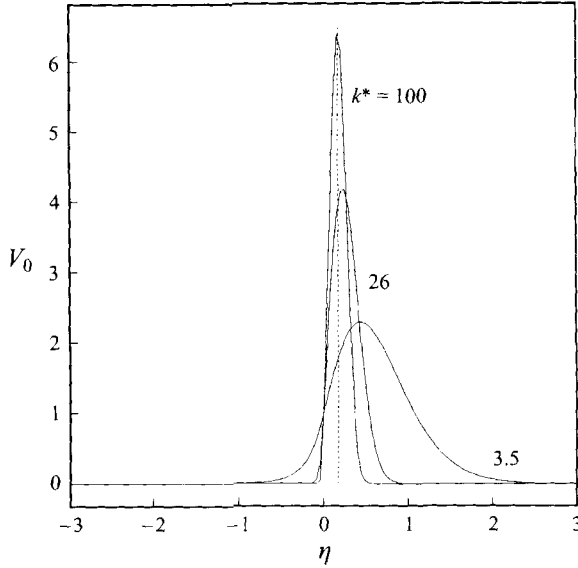
FIGURE 6. First inviscid mode for $k^* = 3.5$, $k^* = 26$ and $k^* = 100$ (the theoretical location of vortex shown as a vertical dashed line).

the unstable mode of the right-hand branch shown in figure 2 and the unstable modes of the inviscid régime shown in figure 4, we see that the growth rate plateaus between the inviscid régime and right-hand branch of the neutral curve. This mimics the Taylor problem in which, at leading order, the most unstable mode is not well defined. On the other hand, in the Görtler problem there is a class of modes with distinctly higher growth rates within this régime, as identified by Denier *et al.* (1991). We have thus verified that the mixing layer must curve into the faster stream in order to be unstable to longitudinal inviscid centrifugal instabilities. This is equivalent to the concave curvature condition for Görtler vortices.

We now show that the inviscid solutions in the limit $k^* \to \infty$ match with the viscous right-hand branch solutions as $\lambda^* \to 0$. We begin by first plotting in figure 6 the inviscid eigenfunctions $V_0$ for the Tanh model verses $\eta$ for three wavenumbers $k^* = 3.5$, $k^* = 26$ and $k^* = 100$. Note that as $k^*$ increases, the structure shrinks to a thin layer, consistent with the asymptotic solution for the right-hand branch. To begin the matching process, we first set $k^* = \epsilon^{-1}$ and take the limit $\epsilon \to 0$. Let $\eta_b$ be the location of the mode, and set

$$\eta = \eta_b + \delta \xi$$

where $\delta = \delta(\epsilon)$. We now expand the quantities

$$\beta^* = \beta_0 + \delta \beta_1 + \delta^2 \beta_2 + \cdots, \qquad f = f_b + \delta \xi f_b' + \tfrac{1}{2} \delta^2 \xi^2 f_b'' + \cdots.$$

Substitution into equation (4.1) yields the conditions

$$\beta_1 = 0, \qquad f'''f' - (f'')^2 = 0 \quad \text{at} \quad \eta = \eta_b.$$

The first condition shows that as $k^* \to \infty$ the growth rate tends to a constant value ($\beta_0 = (-f''/f')^{1/2}$ and this is consistent with the value obtained from (3.3) by setting $\lambda = 0$), refer to figure 4, whilst the second condition defines the location of the layer (this is shown in figure 6 as a vertical dashed line). The eigenfunction satisfies
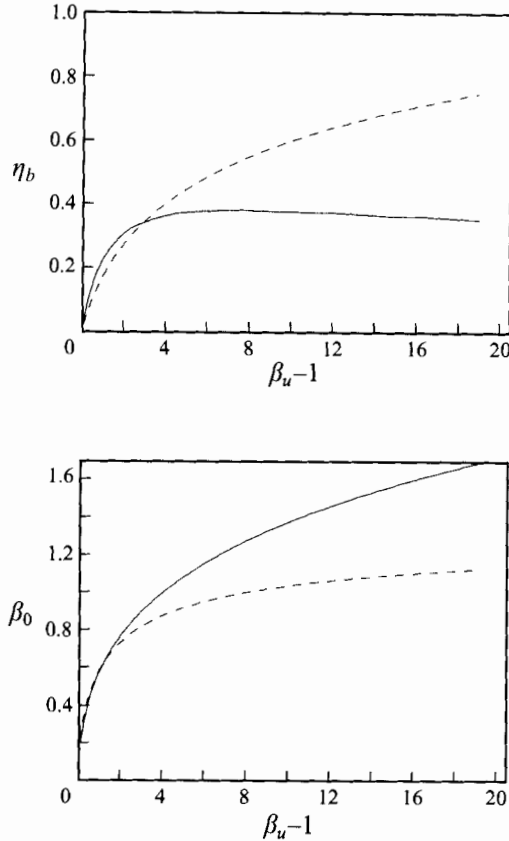
FIGURE 7. Variation of location of the most unstable mode ($\eta_b$) and its growth rate ($\beta_0$) with $\beta_u - 1$ (dashed lines represent the Tanh results and solid lines the Lock results).

a parabolic cylinder equation which matches with the viscous right-hand branch provided the choices $\epsilon = G^{-1/4}$ and $\delta = O(\epsilon^{1/2})$ are made.

We shall now discuss the effect of changing $\beta_u$ on the above structure. As with the right-hand branch problem it is possible to determine analytic solutions for the Tanh model. The solutions for $\eta_b$ and $\beta_0$ are given by

$$\eta_b = \operatorname{arctanh} \left( \frac{\beta_u + 1 - 2\beta_u^{1/2}}{\beta_u - 1} \right)$$

and

$$\beta_0 = \sqrt{2} \frac{\beta_u^{1/2} - 1}{(\beta_u - 1)^{1/2}}.$$

The value of $\eta_b$ (that is the location of the most unstable mode) interestingly corresponds to the point at which $\bar{u} = \beta_u^{1/2}$. The values obtained for $\beta_0$ (both numerically and analytically) match exactly with those from the right-hand branch calculation with $\lambda^* \to 0$. Figure 7 shows the variation of $\eta_b$ and $\beta_0$ with $\beta_u - 1$ (dashed line Tanh, solid line Lock). As with the right-hand branch calculation the location of the mode comes back in towards the centre of the layer; again this is probably due to the more realistic thinning of the Lock profile.

## 5. Numerical methods used to solve (2.1)

The governing equations are parabolic, and thus are solved using a marching procedure in the downstream direction. This makes the whole process orders of magnitude less expensive that the corresponding elliptic problem. The numerical methods used here are taken from Otto & Denier (1996) modified for the mixing layer. The equations are discretized in the downstream coordinate using a Crank–Nicholson scheme, and a standard second-order finite difference technique is used in the normal coordinate. This yields a coupled penta-diagonal and tri-diagonal system which is inverted using techniques detailed in Otto & Bassom (1993). This involves the entire system being inverted using a fairly complicated Thomas algorithm, which serves to retain more of the nature of the system, and hence makes the scheme slightly more implicit than if the penta and tri systems are solved individually. In order to resolve the detail at the centreline, an algebraically stretched grid is used in the normal coordinate, with outer limits at $\pm 40\,(x)^{1/2}$. We chose to solve the problem using the similarity variables, and thus the grid naturally spreads to resolve the layer.

An initial condition was imposed at a streamwise location, $\bar{x}$ say, of the form

$$\tilde{U} = \left(\mathcal{U} + 2\,(\eta - \tilde{\eta})^2\right) e^{-(\eta - \tilde{\eta})^2}, \qquad \tilde{V} = 0 \tag{5.1}$$

where $\tilde{\eta}$ in some sense is the centre of the imposed disturbance and $\mathcal{U}$ is another free parameter. In all the calculations contained here $\bar{x} = 20$; the effect of varying this is to shift the neutral curves slightly, refer to Hall (1983). As one would expect, the modes were found to change with $\tilde{\eta}$, but the characteristics coalesced downstream as predicted in Hall (1982) and observed in Hall (1983). Results are also presented for the initial condition given by

$$\tilde{U} = (\eta - \tilde{\eta})^3\,e^{-(\eta - \tilde{\eta})^2}, \qquad \tilde{V} = 0. \tag{5.2}$$

The essential difference is that the modes are now odd functions of $\eta$ about $\tilde{\eta}$. Finally we consider an initial condition which provides an initial component of streamwise vorticity,

$$\tilde{U} = \left(\mathcal{U} + 2\,(\eta - \tilde{\eta})^2\right) e^{-(\eta - \tilde{\eta})^2}, \qquad \tilde{V} = (\eta - \tilde{\eta})^3\,e^{-(\eta - \tilde{\eta})^2}. \tag{5.3}$$

As the modes progress downstream we monitor the evolution using the energy measure in physical space

$$\mathscr{E}(x) = \int_{\eta = -\infty}^{\eta = \infty} \tilde{U}^2 \mathrm{d}\eta = \frac{1}{(2x)^{1/2}} \int_{y = -\infty}^{y = \infty} \tilde{U}^2 \mathrm{d}y$$

and define the spatial growth rate as

$$\sigma(x) = \frac{\mathscr{E}_x}{\mathscr{E}} + \frac{1}{2x}.$$

We are largely interested in determining the location where the modes start to grow. In a physical problem, some distance downstream of this location it is likely that nonlinear effects will come into play. Hence we shall produce neutral curves of $G_x$ versus $k_x$ (both defined in §3), where a neutral point is defined as where the real part of $\sigma$ changes sign (in this case $\sigma$ is always real; if we were to consider temporal oscillations to the problem this would result in less unstable modes, as shown in Otto & Denier 1996).

The basic state is taken to be the Lock model and is generated using a fourth-order Runge–Kutta scheme in conjunction with a two-dimensional secant method. The
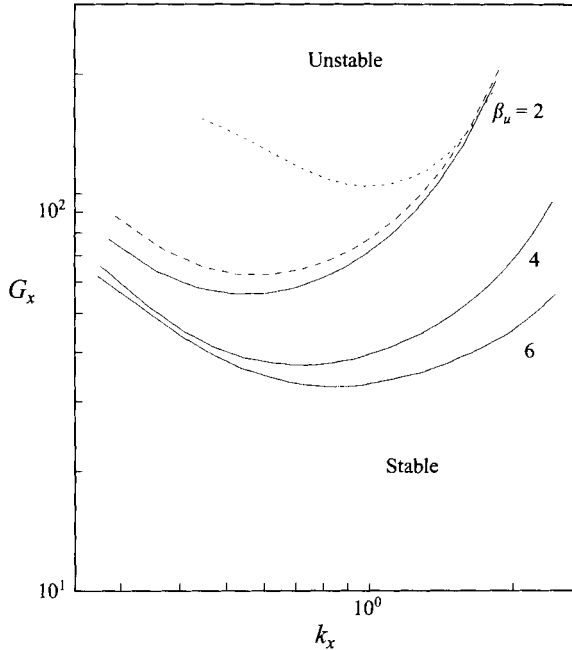
FIGURE 8. Neutral curves for $G = 1/20$, $\chi = (x/\bar{x})^{1/2}$: initial conditions (5.1) (solid curves), with $\beta_u$ = 6, 4 and 2; initial conditions (5.2) with $\beta_u = 2$ (upper dashed curve), and initial conditions (5.3) with $\beta_u = 2$ (lower dashed curve).

mean flow quantities are constructed from the similarity forms at each station rather than marching the boundary layer equations forward. We shall now discuss the results of our calculations.

## 6. Results

In this section we present results concerning Görtler modes with wavelengths commensurate with the mixing layer's thickness and for order-one Görtler numbers. It is clear that there are no local approximations which can deal with this problem other than predicting the far downstream behaviour. The majority of 'local' approximations use the argument that since the flow evolves over longer scales in the streamwise coordinate than in the normal layer variable, the streamwise derivative of $\bar{u}$, and hence $\bar{v}$, is zero (from continuity). This argument allows one to use a normal mode analysis, with $\tilde{U} = \hat{U}e^{i\alpha x}$, where $\alpha$ is the eigenvalue. Whilst this is suitable for the inviscid modes in which the streamwise evolution is on a far shorter scale than the boundary layer evolves on, it is not so in the Görtler problem.

We solved equation (2.1) subject to the initial conditions (5.1) with $\mathcal{U} = 5$ and $\tilde{\eta} = 5$. Note that the disturbance was placed above the centreline. Similar results were obtained for the cases $\tilde{\eta} = 0$ and $\tilde{\eta} = -5$ and are not presented here. The curvature is taken to have the form $\chi = (x/\bar{x})^{1/2}$ and the Görtler number was taken to be $G = 1/20$. In figure 8 we plot $G_x$ versus $k_x$ for $\beta_u = 2$, 4 and 6. Note that as $\beta_u$ increases (i.e. greater disparity between the free-stream speeds), the right-hand branch moves to the right, consistent with the analysis presented in §3. Also note that as the value of $\beta_u$ increases, the minimum of $G_x$ decreases, implying that in general the modes will become unstable earlier. This is found to be true for other initial
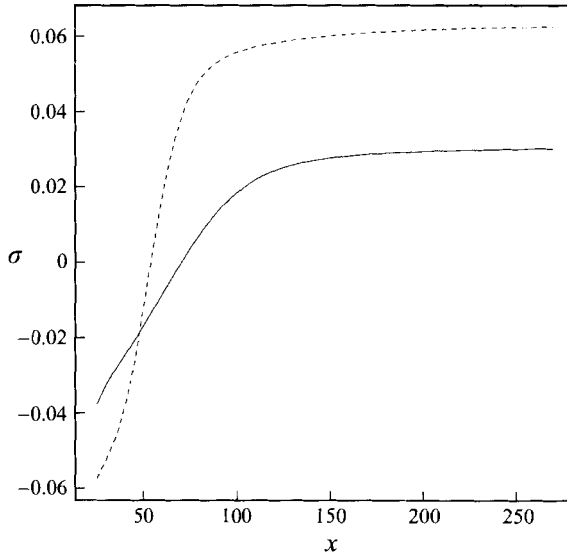
FIGURE 9. Growth rates for $\beta_u = 6$ (dashed) and $\beta_u = 2$ (solid) optimized for $k$
($k = 0.071$ for $\beta_u = 2$ and $k = 0.121$ for $\beta_u = 6$).

conditions. Here, as in Hall (1983) and Otto & Denier (1996), the centre and left-hand parts of the neutral curve are dependent on the particular initial conditions chosen. For comparison, we also show in figure 8 results using the odd initial conditions (5.2) with $\beta_u = 2$ and also for the condition with a non-zero component of streamwise vorticity, (5.3). We note that for all these conditions the neutral curves coalesce on the right-hand branch; however the minima and left-hand branches are strongly dependent on the initial conditions. In figure 9 we plot the growth rate $\sigma(x)$ as a function of $x$ for the initial condition (5.1) with $\mathscr{U} = 5$, $\tilde{\eta} = 5$, for $\beta_u = 6$ (dashed curve) and $\beta_u = 2$ (solid curve). In each case, the wavenumber $k$ chosen corresponds to the respective minimum of the neutral curve, as shown in figure 8: for $\beta_u = 6$, $k = 0.121$ and for $\beta_u = 2$, $k = 0.071$. Note that the mode corresponding to the case $\beta_u = 6$ becomes unstable earlier and has a larger growth rate than the case $\beta_u = 2$.

To illustrate the streamwise structure of the Görtler modes, we plot in figure 10 the spanwise vorticity

$$\omega_{(z^*)}^* = -\frac{\partial u^*}{\partial y^*} + \frac{\partial v^*}{\partial x^*},$$

$$\omega_{(z)} = -\bar{u}_y + \Delta \left(-\tilde{U}_y\right) e^{ikz} + O(\text{Re}^{-1/2})\cdots$$

(an asterisk denotes a dimensional quantity) at one downstream location and with $\Delta = 0.001$. The initial conditions and parametric values are the same as in figure 9 for $\beta_u = 2$. It is worth noting that the vorticity occupies virtually the whole layer (as can be seen by comparison with the accompanying profile). This plot is obviously artificial since a finite-amplitude copy of an infinitesimal mode has been superimposed on the flow; however it does show that this vortex structure could play a significant role in mixing enhancement.

We remark here that the choices of $\mathscr{U}$ and $\tilde{\eta}$ are in a sense arbitrary since the starting condition is artificial and is not derived from any rigorous analysis. We shall not try to identify the most unstable mode for the order-one Görtler number
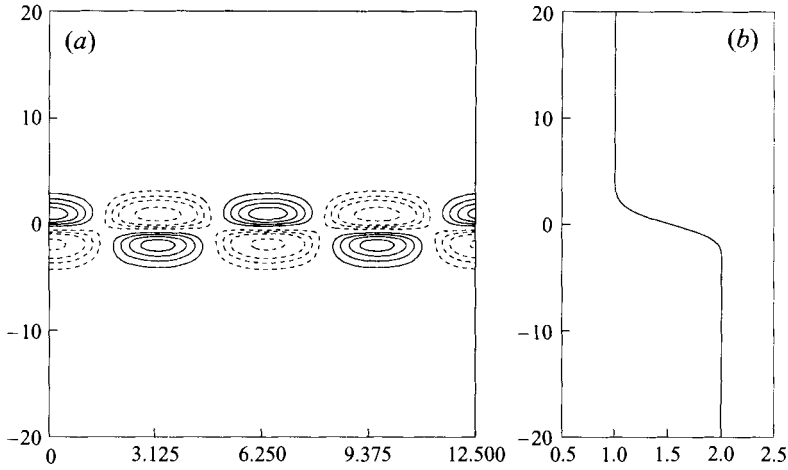
FIGURE 10. (*a*) Spanwise vorticity at $x = 520$ from initial conditions (5.1) as used in figure 8 for $k = 0.071$, $G = \frac{1}{20}$, $\chi = (x/\bar{x})^{1/2}$, and $\beta_u = 2$. (*b*) The streamwise component of the basic velocity.
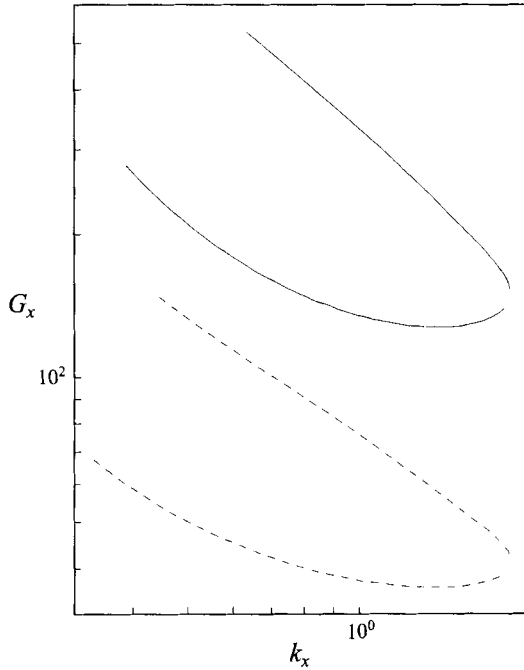


FIGURE 11. Neutral curves for $G = -1/20$ and $\chi = (x/\bar{x})^{1/2}$ (solid) and $\chi = 1$ (dashed).

calculation. In these kinds of calculations it is not at all obvious how one would define the most unstable mode. Unfortunately it is not just a matter of finding the mode with the greatest growth rate, since this quantity varies downstream. It is our intention to provide information concerning the receptivity of this situation in the near future. In the article of Hall (1990) the problem of free-stream receptivity of Görtler vortices within a boundary layer was considered and, by using similar techniques, we intend to demonstrate the receptivity of the situation considered herein to free-stream disturbances.
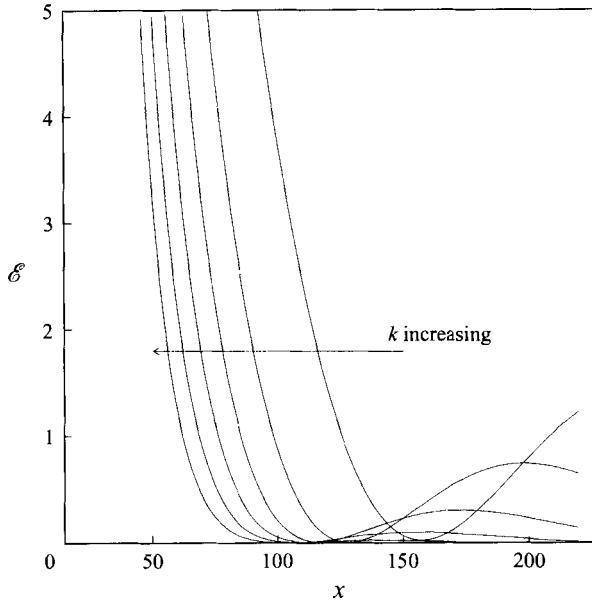
FIGURE 12. Energy $\mathscr{E}$ for $G = -1/20$, $\chi = (x/\bar{x})^{1/2}$
for $k = 0.031, 0.036, 0.041, 0.046, 0.051$ and $0.056$.

In figure 11 we plot the neutral curves for the case $G = -1/20$, $\beta_u = 2$ and $\chi = (x/\bar{x})^{1/2}$ (solid) and $\chi = 1$ (dashed). The initial condition used in these calculations was taken to be (5.1) with $\tilde{\eta} = 0$ and $\mathscr{U} = 5$. The negative Görtler number corresponds to the case for which the centreline curves into the slower stream. Note the somewhat surprising result of the existence of an unstable band for small spanwise wavenumbers. For wavenumbers larger than a critical value, the flow is stable for all Görtler numbers. This is consistent with the analysis presented in §§3 and 4, as well as the recent work by Liou (1994) and Hu et al. (1994).

Thus, all the high-Görtler-number modes are stable except for those in the neighbourhood of the left-hand branch. We are not suggesting that these modes will be observed in a physical problem, merely that it is important to include all the physics of a problem since these modes would be missed by the parallel flow approximations. In figure 12 we show the energy $\mathscr{E}$ associated with these modes for the case $\chi = (x/\bar{x})^{1/2}$ and for several wavenumbers. As $k$ decreases the modes become more unstable, suggesting that the most linearly unstable mode will have a very long spanwise wavelength. It would be interesting to explore the analysis of Choudhari, Hall & Streett (1994) for this problem. In that article the receptivity of long-wavelength modes is discussed and the modes were found to operate within a triple-deck type structure. The other information that can be gleaned from figure 12 is that the energy does not return its original value. This is probably the reason why these modes have not been reported in the experimental literature.

## 7. Concluding remarks

This study has demonstrated that the curved incompressible mixing layer can support centrifugal modes of instability which take the form of longitudinal vortices if the mixing layer curves towards the faster stream. As far as we are aware this is the first work which investigates the evolution of modes in curved mixing layers where
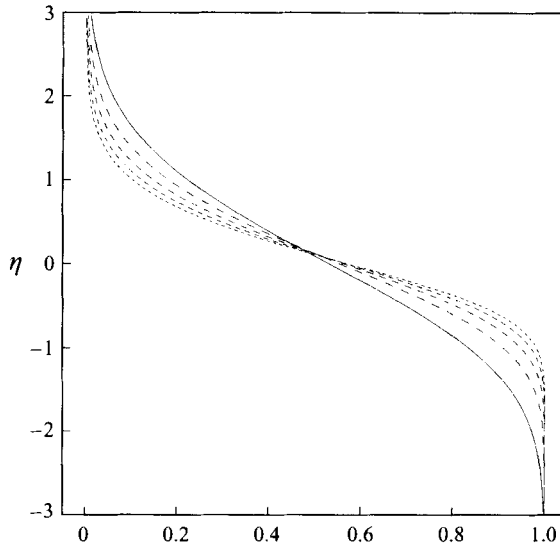
FIGURE 13. $(\bar{u} - 1)/(\beta_u - 1)$ for $\beta_u = 2, 4, 6, 8$ and $10$.
$\beta_u = 2$ corresponds to the solid line and $\beta_u = 10$ the dotted line

the wavelengths are comparable with the layer's thickness and the Görtler number is of order one. In order to determine the stability of a given flow it is crucial to include many of the real flow features, for instance the spreading of the mixing layer and the presence of a normal velocity. The extra parameters that this incurs make a parametric study enormous. However, we have shown that by solving the full linear parabolic governing equations, we could predict a given mode's characteristics. In addition, we have shown that as the modes develop downstream, they conform to a far downstream asymptotic structure. It is in this régime that the parallel flow approximation could be used; however it is then irrelevant, owing to the short scales over which the modes develop. We were also able to show by asymptotic techniques and by direct solution, that as the disparity between the stream speeds increased, the right-hand branch moved to the right, so that more modes became unstable.

In §3 it was shown that as the wavenumber decreased from its $O(G^{1/4})$ value (which corresponds to the right-hand branch of the neutral curve), the growth rate of the modes tended to a constant multiplied by $G^{1/2}$. Similarly in §4 we showed that as the wavenumber increased in the inviscid régime, the growth rate asymptoted to the same value. Thus, there is a direct matching between the two problems and the most unstable mode is not uniquely defined (at least to leading order). It is, however, still possible to identify the most unstable linear mode in these cases and the interested reader is referred to Otto & Bassom (1994) for a discussion of the Taylor case. It is interesting to note that it is possible to show that as the stream speed ratio increases the location of the right-hand branch moves further to the right, implying that a greater range of wavenumbers will be unstable. We also showed in §§3 and 4 that the neutral mode and the most unstable mode were found to remain in the neighbourhood of the centreline as the stream speed ratio increased. We conjectured that this was due to the fact that the mixing layer effectively thins as the stream speed ratio increases. In figure 13 we show $(\bar{u} - 1)/(\beta_u - 1)$ for a variety of values of $\beta_u$ (for the Lock profile) and one can clearly see that as $\beta_u$ increases the extent of the layer narrows.

Finally, we also demonstrated that the case in which the centreline curved into the slower stream can also support centrifugal instabilities. It should be stressed that these modes grow for far reduced streamwise distances and do not seem to grow beyond their initial amplitudes (refer to figure 12) and thus are unlikely to be seen within experimental configurations. However, we have shown that the most unstable modes have very small wavenumbers, and their receptivity may be important, Choudhari *et al.* (1994). This result does not contradict the asymptotic work, since we still predict that the inviscid and right-hand branch modes are stable. It will be interesting to extend this study to compressible and three-dimensional mixing layers.

## REFERENCES

CASTRO, I. P. & BRADSHAW, P. 1976 The turbulence structure of a highly curved mixing layer. *J. Fluid Mech.* **73**, 265–304.

CHOUDHARI, M., HALL, P. & STREETT, C. L. 1994 On the spatial evolution of long–wavelength Görtler vortices governed by a viscous–inviscid interaction, Part 1: The linear case. *Q. J. Mech. Appl. Maths* **47**, 207–229.

DENIER, J. P., HALL, P. & SEDDOUGUI, S. 1991 On the receptivity problem for Görtler vortices: vortex motion induced by wall roughness. *Phil. Trans. R. Soc. Lond.* A **335**, 51–85.

DRAZIN, P.G. & REID, W.H. 1979 *Hydrodynamic Instability.* Cambridge University Press.

GÖRTLER, H. 1940 On the three dimensional instability of laminar boundary layers on concave walls. *NACA Tech. Mem.* 1375.

HALL, P. 1982 Taylor–Görtler vortices in fully developed or boundary layer flows. *J. Fluid Mech.* **124**, 475–494.

HALL, P. 1983 The linear development of Görtler vortices in growing boundary layers. *J. Fluid Mech.* **130**, 41–58.

HALL, P. 1990 Görtler vortices in growing boundary layers: the leading edge receptivity problem, linear growth and the nonlinear breakdown stage. *Mathematika* **37**, 151–189.

HU, F. Q., OTTO, S. R. & JACKSON, T. L. 1994 On the stability of a curved mixing layer. In *Proc. ICASE Workshop on Transition, Turbulence and Combustion, 1993* (ed. T. B. Gatski, M. Y. Hussaini & T. L. Jackson), pp. 107–116. Kluwer.

KARASSO, P. S. & MUNGAL, M. G. 1990 An experimental study of curved mixing layers: flow visualization using volume rendering. *Center for Turbulence, Annual Research Briefs*, pp. 195–201.

KARASSO, P. S. & MUNGAL, M. G. 1991 Mixing measurements of straight and curved shear layers. *Center for Turbulence, Annual Research Briefs*, pp. 343–348.

LEBOEUF, R. L. 1991 Progress toward identification of streamwise vorticity meander in a plane mixing layer. *Center for Turbulence, Annual Research Briefs*, pp. 349–354.

LIOU, W. W. 1994 Linear Instability of curved free shear layers. *Phys. Fluids* **6**, 541–549.

LOCK, R. C. 1951 The velocity distribution in the laminar boundary layer between parallel streams. *Q. J. Mech.* **4**, 42–57.

MARGOLIS, D. P. & LUMLEY, J. L. 1965 Curved turbulent mixing layer. *Phys. Fluids* **8**, 1775–1784.

MICHALKE, A. 1964 On the inviscid instability of the hyperbolic-tangent velocity profile. *J. Fluid Mech.* **19**, 543–556.

MICHALKE, A. 1965 On spatially growing disturbances in an inviscid shear layer. *J. Fluid Mech.* **23**, 521–544.

OTTO, S. R. & BASSOM, A. P. 1993 An algorithm for solving the viscous equations arising in the stability of three-dimensional centrifugal instabilities. *ICASE Internal Rep.* 38.

OTTO, S. R. & BASSOM, A. P. 1994 The effect of crossflow on Taylor vortices. *Q. J. Mech. Appl. Maths* **47**, 323–339.

OTTO, S. R. & DENIER, J. P. 1996 The effect of pressure gradients and three–dimensional flows on Görtler vortices. *J. Fluid Mech* (submitted).

PLESNIAK, M. W., MEHTA, R. D. & JOHNSTON, J. P. 1994 Curved two–stream turbulent mixing layers: three–dimensional structure and streamwise evolution. *J. Fluid Mech.* **270**, 1–50.

TAYLOR, G.I. 1923 Stability of a viscous liquid contained between two rotating cylinders. *Phil. Trans. R. Soc. Lond.* A **223**, 289–343.

WANG, C. 1984 The effects of curvature on turbulent mixing layers. PhD thesis, California Institute of Technology.

WYNGAARD, J. C., TENNEKES, H., LUMLEY, J. L. & MARGOLIS, D. P. 1968 Structure of turbulence in a curved mixing layer. *Phys. Fluids* **11**, 1251–1253.